Spreading of Aqueous Liquids in Unsized Papers is by Film Flow

R.J. ROBERTS, T.J. SENDEN, M.A. KNACKSTEDT and M.B. LYNE

We use cryo-scanning electron microscopy to visualize the penetration of a wetting fluid into various bleached softwood kraft papers. The results indicate that the fluid movement is due primarily to the advance of the wetting fluid in the form of bulk liquid films along channels formed by fibre overlaps. This is in contrast to the common description of fluid penetration, where the primary flow mechanism is based on the bulk filling of pores. The channels formed by fibre overlaps are shown to form a highly interconnected dense network of flow paths which efficiently transport the wetting fluid. We calculate the flow rates associated with penetration along a number of potential flow paths within the fibre web. The experimentally observed penetration rate is consistent with a film flow process through interfibre channels which is significantly slower than a penetration process dominated by meniscus flow through pores.

Nous utilisons le cryo-microscope électronique à balayage pour visualiser la pénétration des fluides mouillants dans divers papiers kraft blanchis de résineux. Les résultats indiquent que le mouvement du fluide est attribuable principalement au fluide mouillant sous forme de pellicule liquide le long des canaux formés par le chevauchement des fibres, ce qui vient à l'encontre de la description courante de la pénétration du fluide, où le mécanisme de débit primaire est basé sur le remplissage global des pores. Les canaux formés par le chevauchement des fibres forment un réseau dense et interconnecté de voies de circulation transportant efficacement le fluide mouillant. Nous calculons le débit associé à la pénétration le long d'un certain nombre de canaux unidirectionnels potentiels dans la feuille fibreuse. Le taux de pénétration observé en laboratoire est conforme au débit d'une pellicule dans des canaux interfibres qui est significativement inférieur à un processus de pénétration dominé par un ménisque unidirectionnel dans les pores.

INTRODUCTION

The kinetics of capillary penetration of wetting liquids into porous media is of particular interest due to its applications in the paper and textile industries and in printing technologies. An understanding of fluid penetration processes is necessary in understanding all converting processes where contact between paper and fluid plays a role.

The Lucas-Washburn [1,2] theory is used commonly to model the penetration of liquids into porous materials where the rate of penetration is a function of the balance between surface tension forces and viscous drag. The interfacial contact angle is assumed to be constant and the pore morphology is reduced to an equivalent cylindrical pore. It has long been recognized that this is a gross oversimplification of the true morphology of a paper product, which in reality is a material made up of a cellulose fibre matrix, in many cases coated with a consolidated mass of pigment and binder. It has been noted before that important differences exist between penetration of a liquid into a capillary and penetration into a more complex porous medium [3,4]. The development of tools to describe more realistically the pore morphology of porous materials is an emerging discipline of recent interest [5–9].

To gain a better understanding of fluid penetration into paper, one must not only effectively characterize the morphology of the pores within the fibre web. One must also obtain a fundamental understanding of the physical processes which affect fluid movement and fluid–solid interactions during fluid penetration. Penetration models, including the classical Lucas-Washburn equation, assume that the major mechanism for fluid penetration into paper is via capillary transport within pores. Eklund and Salminen [10] considered a number of water transport mechanisms including liquid capillary transport through pores, diffusion of vapour, surface diffusion in pores and intrafibre flow; they observe that bulk capillary transport in pores remains the most important mechanism.

Recent work [11] has included the study of inertial effects on fluid penetration. In all descriptions of fluid penetration, pores are considered to be occupied by a single fluid and the pore-filling mechanism is by meniscus movement down the pore centre.

JPPS

R.J. Roberts and T.J. Senden
Dept. Applied Mathematics
Res. School Phys. Sci. and Engin.
Australian National Univ.
Canberra ACT 0200, Australia
M.A. Knackstedt
Dept. Applied Mathematics
Res. School Phys. Sci and Engin.
Australian National Univ.
Canberra ACT 0200, Australia
School Petroleum Engin.
Univ. New South Wales
Sydney, NSW 2052, Australia
(mark.knackstedt@anu.edu.au)
M.B. Lyne
International Paper
Corp. Res. Center
1422 Long Meadow Road
Tuxedo, NY, USA
10987

In a previous paper [12], some of the present authors performed an experimental investigation of droplet penetration into idealized etched two-dimensional porous networks. Results showed that, during the penetration of a wetting fluid into a porous network, there is a competition between an advancing and swelling bulk wetting film and capillary transport in the pores. In this paper, we extend the work to a study of fluid penetration into 3-D paper fibre webs. We use cryo-scanning electron microscopy (cryo-SEM) to visualize the fluid phase as it penetrates into a range of paper types. Paper types studied include fully bleached softwood kraft paper and a number of saturating kraft papers used as low-pressure melamine laminates. We observe that the fluid flow cannot be characterized by an advancing wetting front moving along the bulk of the pores. We observe a large and diffuse partially saturated zone, where fluid occupies only the edges of pores and forms films along channels formed by fibre overlaps. The results indicate that the fluid movement is due primarily to the advance of the wetting fluid in the form of bulk liquid films along these channels. This is in contrast to the common description of fluid penetration, where the primary flow mechanism is based on the bulk filling of pores.

To understand the observed behaviour, we consider the 3-D structure of a paper web. We observe that a number of potential flow paths for the wetting fluid exist within the fibre network at different length scales; these include flow within the pores, flow along channels formed by fibre overlap, flow along the fibre indentations caused by fibre collapse during pressing and fibre roughness, and intrafibre flow. We define the relevant length scale associated with each flow path and discuss the continuity and representative morphology of the pathways. A description of pore-scale mechanisms for fluid penetration is given for the pore morphologies associated with each potential flow path. We find that the continuous displacement of a meniscus along bulk pores is highly unlikely due to the presence of discontinuities in the pore morphology. We show that a preferential displacement mechanism is via film flow. The channels formed by fibre overlaps are shown to form a highly interconnected and dense network of flow paths which efficiently transport the wetting fluid. We calculate the flow rates associated with penetration along each transport pathway; the experimentally observed penetration rate is consistent with a film flow process through channels and significantly slower than a penetration process dominated by meniscus-driven flow through pores.

EXPERIMENTAL METHODS

The experimental goal was to visualize the transport mechanism of a wetting fluid during fluid penetration. The speed of imbibition and the resolution required to study the wetting sequence at the fibre scale is experimentally challenging. To maintain good fibre and liquid discrimination, cryo-SEM was preferred for this study. As cryo-SEM can maintain the samples at −165°C during the imaging process, it avoids problems which occur in conventional SEM where hydrated materials undergo shrinkage and distortion due to the high-vacuum environment. Providing an imbibition process is frozen quickly enough, and maintained suitably cold, the actual fluid distribution can be observed.

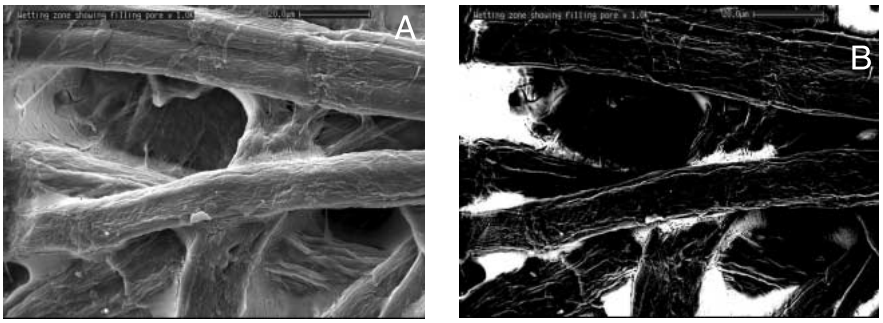

Fig. 1. An example of an SEM image of fluid penetration into kraft paper in (A) secondary electron mode and (B) backscattered mode.

A Cambridge Instruments S360 Stereoscan SEM fitted with a high brightness LaB_6 electron source, a backscattered electron detector and a cryogen transfer chamber was used in the study. The paper samples used included fully bleached softwood kraft laboratory paper containing no sizing or filler material (International Paper), an 80 g/m^2 laser copy paper (Australian Paper), as well as a number of saturating kraft papers used for the production of low-pressure melamine panels. Samples, 15 × 5 mm, were fixed to a standard specimen holder with tissue freezing medium made up of equal proportions of G. 303 Colloidal Graphite (Aquadag) (Agar Aids) and Tissue-Tek OCT Compound 4583 embedding medium (Miles Scientific). Approximately 20 μL of 2 mol/L cesium iodide aqueous solution was applied to each sample and plunged immediately into a semifrozen slush of nitrogen at a temperature around −230°C. This ensures rapid and total freezing of the specimen within 0.5 s. As the total imbibition time for the droplet was ~3 s, in every case bulk liquid in the form of a frozen droplet remained on the surface of the paper.

Reduction of artifacts is crucial and has been discussed by Robards and Sleytr [13]; in particular, the rapid freezing of the sample. The use of N_2 slush results in a cooling rate of over 10 000 K /s which will ensure a rapid transition between the homogeneous nucleation point of 230 K and the recrystallization point at 130 K, thus avoiding crystallization of water. Based on this methodology, we are confident that the fluid phase remains undisturbed and a dynamic snapshot of droplet imbibition is observed. Low magnifications and accelerating voltages (15 kV) also helped reduce the production of artifacts.

When the snap-frozen samples were then inserted into the chamber of the SEM, a light frost frequently decorated the sample as a result of condensation of atmospheric moisture. To remove this adventitious ice, the sample was warmed briefly under vacuum to −80°C. By monitoring the secondary electron image during this process, selective sublimation of the frost was possible. The sample was then cooled back to −165°C and coated with an ~10 nm layer of gold before being returned to the SEM chamber. The samples were maintained at approximately −165°C during examination and imaged in both secondary and backscattered electron modes. Magnifications varied from X60 which enabled the full droplet area to be imaged to over X1500 to obtain high-definition images of individual pores and channels.

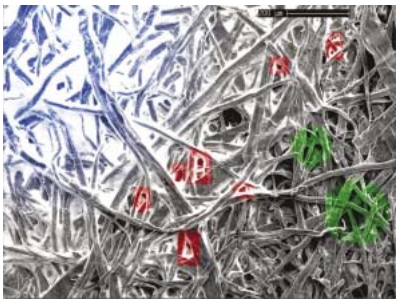

Fig. 2. Low-magnification image showing the fluid configuration at the paper surface. We observe that near the droplet (upper left of the image) a region of saturation exists (shaded blue). The remaining regions exhibiting the presence of fluid are partially saturated. Regions in red show where pores exhibit partial filling. Green regions illustrate where the surface pores diverge to large openings.

The CsI solution gave excellent contrast against fibres in backscattered electron mode. Unlike a number of other microscopy stains, CsI solutions did not chromatographically separate. Figure 1 shows the same region imaged in A) secondary electron mode and B) backscattered mode. The colouration shown in successive electron micrographs is derived directly from overlaying a colourized backscattered image with the secondary image to highlight the morphologies of liquid imbibition.

EXPERIMENTAL RESULTS

In Fig. 2, we show a low-magnification image which illustrates the typical penetrating

fluid configuration at the paper surface emanating from the drop edge (upper left corner) radially outwards. Two regions can be observed in the image. Near the droplet edge, we observe a region where the surface pores are completely saturated; this region extends ~500 μm from the drop edge (blue shade). The remaining region is only partially saturated by the penetrating fluid. The degree of saturation decreases as one moves further from the drop edge, and at the outer regions of the partially saturated zone we see that the penetrating fluid is present only in the form of films in the regions between the fibres. We observe large pores that remain unsaturated in the midst of smaller filled pores.

In Fig. 3, we show the typical fluid distribution in the midst of the saturated zone. One observes that pores at the surface are not all filled, and fibres at depth are still visible to the surface. We also note that the fluid does not tend to wet the upper surface of the paper fibre; the fluid interface instead seems to wet the fibre edges preferentially and becomes pinned along the fibre edge.

In Fig. 4, we show a higher resolution image of a fluid configuration just inside the boundary of the partially saturated zone. We again note that the fluid fills primarily the pores which lie between the edges of fibres (red shading in Fig. 4) and do not wet the upper fibre surface. One also notes the presence of films along channels formed by fibre overlap (blue shading) which interconnect many of the filled pores. Finally, we note that the larger surface pores remain unfilled (yellow shading). Some edges of the large pores, however, do exhibit a presence of a liquid wetting film.

As one moves further away from the droplet edge into the partially saturated zone, one observes a number of interesting fluid configurations within the pore space. In Fig. 5, we observe pores completely filled between fibre edges on the left side (red shading), and the presence of seemingly disconnected fluid films along channels formed by fibre overlap scattered throughout the rest of the image (green shading). One also notes a curious fluid configuration (yellow) within a pore lying 3–4 fibres below the paper surface. Here the pore is mostly filled, but a partial disk of air punctures the centre of the pore. Several of these partially filled pores are visible throughout the partially saturated zone (labelled by squares in the low magnification Fig. 2). A closeup of a partially filled pore is given in Fig. 6.

In Fig. 7 we observe a smaller pore (red) with a pore size of ~10 μm completely filled with the wetting fluid and a larger neighbouring pore size of ~20 μm, (green) which exhibits only a presence of films along the edges.

Figure 8 is taken further out from the drop edge. In this region, we observe the wetting fluid present solely as films along channels formed by fibre overlaps (blue) and as films wetting edges and corners of the pore (red).

At the outer edge of the partially saturating zone we observe only film flow along fibre intersections (Fig. 9). We also observe a small amount of flow along the fibre surface roughness and no flow into fibre pits (arrow).

From the experimental results we can conclude that, particularly in the partially saturated zone, film flow is the major mechanism for transport of the wetting fluid. Bulk flow through the pores generally is not observed.

PORE-SCALE MODELLING OF OBSERVATIONS

In this section, we reconcile two-phase flow modelling with the experimental observation that the capillary penetration is associated primarily with the flow of the wetting fluid in the form of bulk liquid films along channels formed by fibre overlaps and is not observed as bulk flow in the pores. We first give a description of the pore morphology for all potential

Fig. 3. The typical fluid distribution in the midst of the saturated zone. One observes that pores at the surface are not all filled and fibres at depth are still visible to the surface.

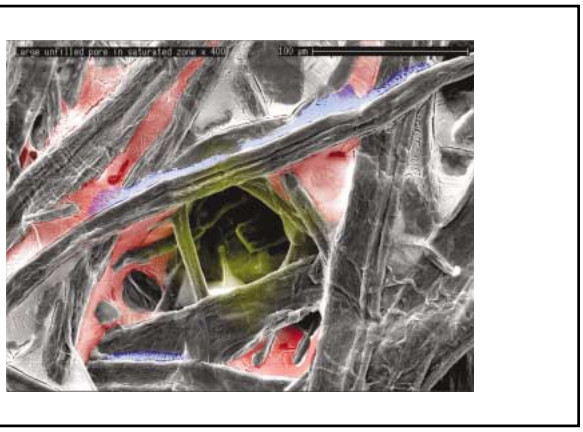

Fig. 4. Higher resolution image of the fluid configuration inside the partially saturated zone.

Fig. 5. Fluid configurations within the partially saturated zone.

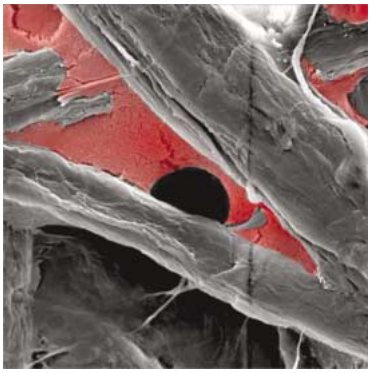

Fig. 6. Closeup of a partially filled pore.

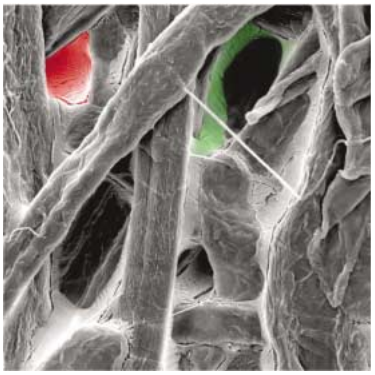

Fig. 7. A small pore (red) with a pore size of ~10 μm completely filled with the wetting fluid and a larger neighbouring pore of size ~20 μm (green) which only exhibits a presence of films along the edges.

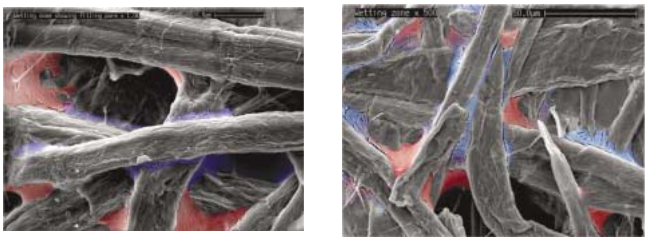

Fig. 8. Two examples of fluid configuration in regions far from the drop edge. Here we observe the wetting fluid is present solely as films along channels formed by overlapping fibres (blue) and as films wetting corners of the pores (red).

flow paths within paper. We then develop a mechanistic description of two-phase flow within each pore morphology. Calculation of the flow rates associated with penetration down fibre- overlap channels is shown to be consistent with the film flow mechanism observed experimentally.

3-D Pore Morphology of Paper

We describe all the potential flow paths for the wetting fluid which exist within the fibre network at different length scales:

— Flow within the bulk pores;
— Flow along channels formed by fibre overlaps;
— Flow along crevices formed by indentations and surface roughness of the fibres; and
— Flow within the intrafibre pores.

In this section, we use the images given in Experimental Results to help describe these various fluid pathways on a paper fibre network, define the length scale associated with these different pathways, and discuss the continuity of the pathways within the sheet.

The size of pore openings within paper is highly variable. A number of different pore sizes are evident at the surface of the paper in Fig. 2 and range from ~20–50 μm. Moreover, the cross-section along a single pore can vary enormously. On penetration down 1–2 fibres into the paper sheet ~10 μm in depth, the pore size suddenly diverges. This pore morphology is evident in the regions shaded green in Fig. 2. One also observes the presence of sharp dislocations in the pore openings when considering a cross-sectional view of a paper sheet; e.g. see figures in [14,15].

Fluid penetrating from small pores at the surface must bridge across large pore openings; bulk penetration of fluids into the pore space is therefore characterized by converging and diverging pores, and pores exhibiting large discontinuities [3]. A schematic of the interfibre pore space is given in Fig. 10A. Due to the large number of fibre overlaps which partition the pore space into many domains, the pores are highly interconnected.

A second potential flow path for the wetting fluid is along channels formed by fibre overlaps. The morphology of these potential flow paths is not simple to determine. Hasuike et al. [14] performed a very careful geometric evaluation of a paper sheet in 3-D based on serial sections at a 2 μm spacing. Statistics on the number of fibres contacting each fibre was calculated for 138 fibres over a (200 μm)^2 area. They observed a huge degree of entanglement and interconnection of fibres. The fibres, and therefore the channels generated via fibre overlaps, lie almost exclusively parallel to the sheet. Hasuike et al. [14] observed minimal migration of fibres perpendicular to the sheet axis. They observed that almost all of the upper and lower surfaces of a paper fibre are in contact with other fibres and they measured ~80 fibres contacting the surface of a fibre for every 1 mm in length. As most fibres are 1 mm in length or longer, this represents a huge degree of fibre entanglement. With respect to the fibre cross-section, they observed often more than 2 fibres bonded to each fibre (Fig. 9 of [14]). This high degree of fibre overlap which is evident in all experiments is sketched schematically in Fig. 10B,C. From these sketches in 3-D and in cross-section, one can identify the pore geometry that emerges due to fibre overlap in Fig. 10D. We observe in cross-section that the overlap of fibres leads to the formation of many small channels. Flow along these channels can be approximated as a corner flow problem down an open channel of angle $\alpha < 90°$. The exact size and channel angle α were not given explicitly in [14], and they are difficult to discern from the SEM images. Based on the cross-sectional images and given that the fibre thickness is ~5–10 μm and the fibre width is ~15 μm, we estimate a channel depth of $r \approx$ 1–3 μm. The flow channels formed by fibre overlap form an extremely dense interconnected network of potential flow paths (see Fig. 10B).

A third potential flow path is based on

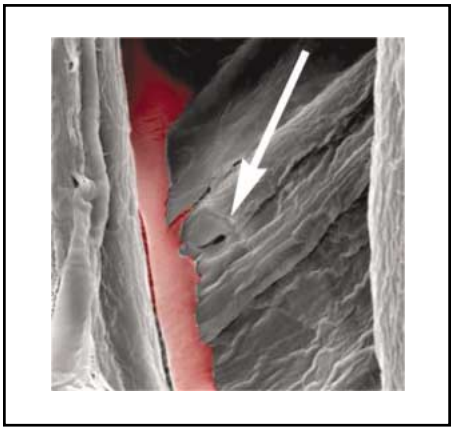

Fig. 9. At the outer edge of the fluid we observe film flow only along fibre intersections. The width of the image is 25 μm.

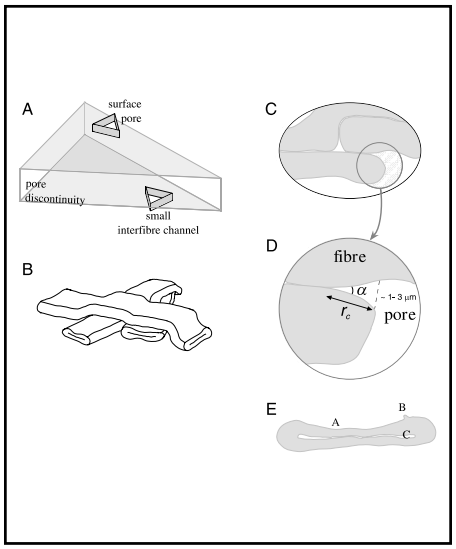

Fig. 10. (A) A schematic of the typical pore geometry in paper sheet: a (small) surface pore opening which opens up to a significantly larger pore. (B) Illustration of the fibre bonding state observed in 3-D; note the large degree of entanglement and interconnection of the fibres. Flow channels formed by fibre overlap and therefore form a highly interconnected pore space. (C) illustrates a typical fibre cross-section picture. The high degree of fibre overlap is reinforced. (D) The open channel pore geometry that is generated by fibre overlap. (E) Illustration of the indentations A and roughness B that are observed on a fibre surface and C the intrafibre pore.

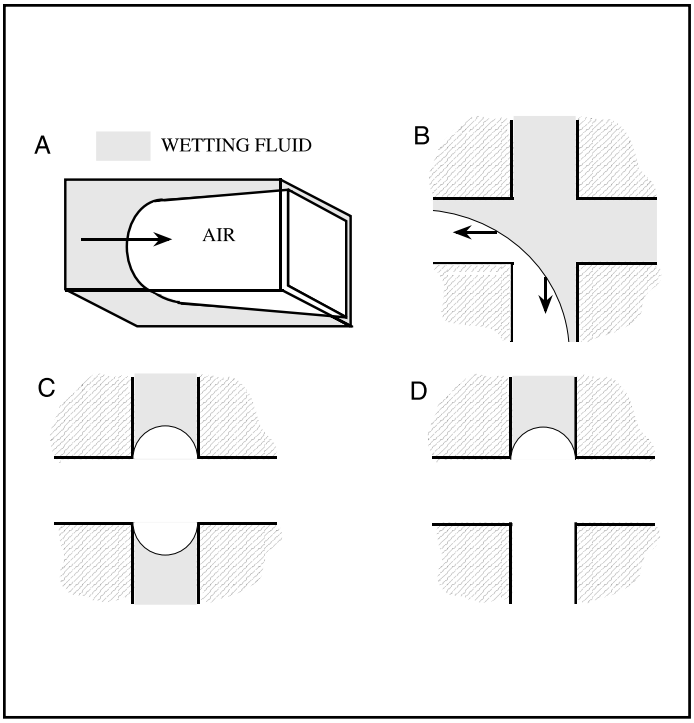

Fig. 11. Interfacial configurations corresponding to different fluid penetration mechanisms; (A) piston displacement, (B–D) penetration across pore boundaries and discontinuities. In case (B), the fluid can continue to advance but, in cases (C) and (D), the fluid configuration will remain stable.

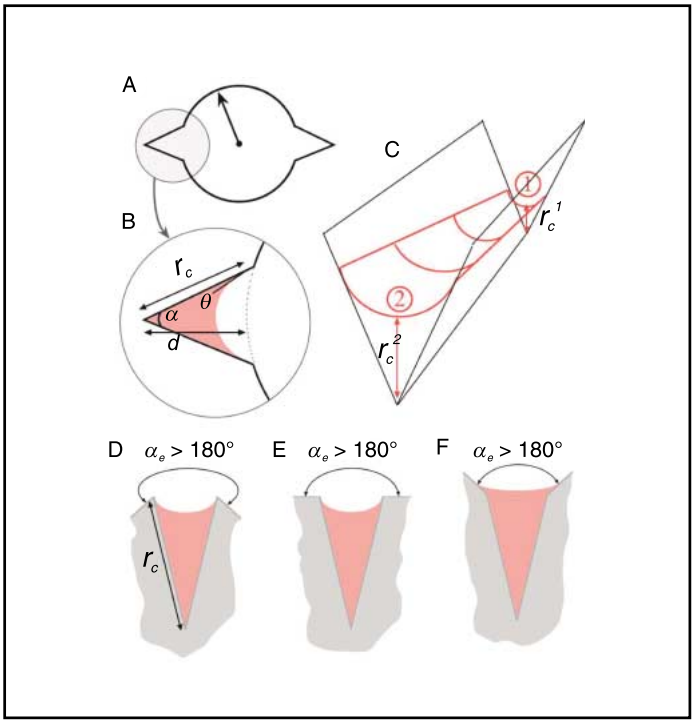

Fig. 12. (A) A simple illustration of a pore with two small fibre overlap channels; (B) gives a more detailed view of the channel geometry. In (C) we illustrate the free penetration of a film along a channel; we illustrate a gradient in the thickness of the film along the edge of uniform cross-section

$$r_c^2 > r_c^1$$

Because of this variation in thickness the capillary pressure at location (1) is greater than at location (2)

$$p_c^1 > p_c^2$$

via Eq. (1). Since the pressure of the non-wetting phase (air) is the same at the two locations the fluid will tend to penetrate along from 2 to 1. (D)–(F) show the fluid configuration at the edge of a channel after filling is complete. In (D,E), $\alpha_e \geq 180°$ and the interface will not thicken beyond the channel depth r_c and will instead remain pinned at the channel/pore edge. In (F), as the effective channel angle $\alpha_e < 180°$, one would observe a continued thickening mechanism.

flow along the roughness or curvature on the surface of a fibre. A typical fibre does not exhibit a purely convex shape, but can exhibit both an indentation due to fibre collapse and roughness in the cross-section (Fig. 10E). One can approximate this flow path by an open channel flow. Here the angle α associated with indentations $\alpha_i > 90°$ and roughness $\alpha_r \approx 90°$ are both large, with the crevice size small, $r <$ 1 μm. These potential flow pathways, which one observes along most fibres, intersect with the fibre-overlap channels; the pathways, however, are quite long, and do not exhibit the strong degree of interconnectivity observed in the fibre-overlap channels.

A schematic of an intrafibre pore is shown also in Fig. 10E. We estimate < 0.5 μm for the intrafibre pore size by consideration of cross-sectional images of the fibre web. The pore geometry can be approximated as eye-shaped. These pores do not form a continuous pore systems throughout the fibre web; the ends of each fibre do not intersect. Flow through a fibre pore would reach the end of the pore and, to continue to penetrate, would need to penetrate across the pores; this is analogous to flow along a small pore reaching a large discontinuity.

Mechanisms of Displacement in Porous Networks

Pore-scale mechanisms observed during penetration of a wetting fluid may be described using the terminology first introduced by Lenormand et al. in 1983 [16]. There are two distinct types of advance. The first is piston-like, where the fluid advances as a meniscus occupying the centres of the pore space. In the second, the wetting fluid flows along crevices in the pore space, filling pores in advance of the wetting front. We illustrate the two types of advance based on simplified pore descriptions. Although the pore-scale morphology of paper is much more complex, these simple illustrations give one a better understanding of the penetration mechanisms observed experimentally.

The simplest type of fluid motion in a network of pores is piston-type motion; the meniscus is inside a channel and the wetting (fluid) phase displaces the non-wetting phase (air) (Fig. 11A). The filling of a network of intersecting channels of variable aspect, as is the case for paper webs (Fig. 10A), is more complex than flow down a single channel.

In particular, the presence of pores at junctions of flow channels and sharp dislocations in the network lead to very different flow processes. As discussed in [16,12], the filling of these junctions and discontinuities depends on the capillary (displacement) pressures associated with meniscus advancement. This includes the fluid distribution within the pores (e.g. the number of neighbouring channels filled with wetting fluid) and the contact angle and pore size [12,16]. The primary result is that only when the majority of pores at a junction are filled with a wetting fluid can the meniscus continue to penetrate via a frontal advance (Fig. 11B). Other configurations where neighbouring pores at the junctions remain filled with non-wetting fluid (air) (Fig. 11C) or the meniscus reaches a discontinuity (Fig. 11D), the fluid configuration remains stable and continued displacement can only take place by a film-flow mechanism. For example, a fluid meniscus advancing down the smaller pores in Fig. 10A, a fluid configuration similar to that illustrated in Fig. 11D, will not advance beyond the junction to the large pore opening (discontinuity) [3]. The principal radii of curvature at a discontinuity are infinite, therefore the capillary pressure or driving force for further advancement is zero.

The only mechanism for fluid to advance beyond discontinuities like those illustrated in Fig. 11C,D is via film flow. If the frontal meniscus cannot advance down a pore, the wetting fluid will flow as a film along the edges of the pores. Based on the illustration in Fig. 10D, we consider a representative pore cross-section that includes a pore of radius R and open channels of depth d (Fig. 12A). A simple schematic

of the channel with a uniform cross-section and partially filled with the wetting fluid is given in Fig. 12B. Assuming the capillary is sufficiently long compared to its diameter, the capillary pressure across the liquid meniscus in the edge can be calculated as

$$P_c = \gamma \cos(\theta + \alpha/2)/r_c \quad (1)$$

where γ is the surface tension, θ is the contact angle of the fluid at the solid interface, α is the opening angle of the crevice and r_c is the distance between the liquid/solid contact lines. This implies that, for fluid to advance down the crevice, $P_c > 0$, $0° \le (\theta + \alpha/2) \le 90°$. As the channels formed by fibre overlaps have $\alpha < 90°$, it can be expected that most wetting fluids will spontaneously penetrate along these flow paths. Progressive penetration of the wetting phase along a channel is driven by the interfacial configuration; if the film is thinner, the curvature of the liquid meniscus in the edge is increased and, consequently, the capillary pressure is higher. Figure 12C illustrates the penetration of the wetting liquid along a channel of depth d formed by the fibre overlaps (similar to that observed experimentally in Fig. 9). If fluid is available the films will continue to thicken until the channel fills completely, $r_c^1 = r_c^2 = d$ in Fig. 12C.

At the channel/pore interface (Fig. 12D–F), depending on the edge configuration, the films will either continue to swell or become pinned. We define an angle α_e as the angle formed by the edges of the pore near the pore/channel interface. If the channel geometry associated with a fibre overlap opens to a flat discontinuity ($\alpha_e = 180°$) or to an angle ($\alpha_e > 180°$), one would expect the fluid interface to be pinned and observe no thickening of the film beyond the channel depth d, ($r_c \le d$), as illustrated in Fig. 12D,E. However, if the opening at the pore edge has an $\alpha_e < 180°$ (Fig. 12F), one may observe continued, albeit slower, film thickening into the pore.

We expect that the typical pore/channel interface will exhibit an angle $\alpha_e < 180°$. From the data of [14], we know that the average number of fibre bonds expressed with respect to the fibre cross-section is ≥2. A cross-sectional view of the pore geometry at the edge of a fibre in cross-section can therefore exhibit channels which lie in close proximity (Fig. 13A,B). Since fibres viewed in cross-section exhibit primarily a convex shape and are aligned perpendicular to the sheet axis, the pore/channel interface is highly likely to exhibit $\alpha_e < 180°$. As shown in Fig. 12F, for a pore/channel interface exhibiting an $\alpha_e < 180°$, the films will continue to thicken beyond the channel edge. The advancement of the wetting fluid via thickening films therefore can lead to the intersection of the menisci in the two channels; configuration (2) in Fig. 13B results. The merged menisci now will accumulate as a growing collar within the channel cross-section and will stop only at a new discontinuity in the pore morphology (configuration 3 in Fig. 13B). This partial pore filling along the edge of a pore via films is observed in several experimental images (e.g. see some regions shaded blue in Fig. 8).

If the pore cross-section is small enough and/or the advancing films within a pore are thick enough, eventually the wetting fluid can come into complete contact with the channel wall and an unstable non-wetting fluid (air) filament is created within the pore which spontaneously thins and snaps off [16]. The wetting fluid now completely fills the pore (Fig. 13C). The experimental images illustrate this mechanism in progress. The partially saturated pores highlighted in Figs. 2 (red shading), 5 (yellow shading) and 6 are all very close to having become completely filled; only one fibre edge remains in contact with the air (non-wetting phase) and the pore exhibits a small circular hole near the pore centre. On continued film advancement the pore would be completely filled. Numerous pores completely filled via film flow are evident in Fig. 2; a close up of a pore that has filled via film flow is shown in Fig. 7 (red shading).

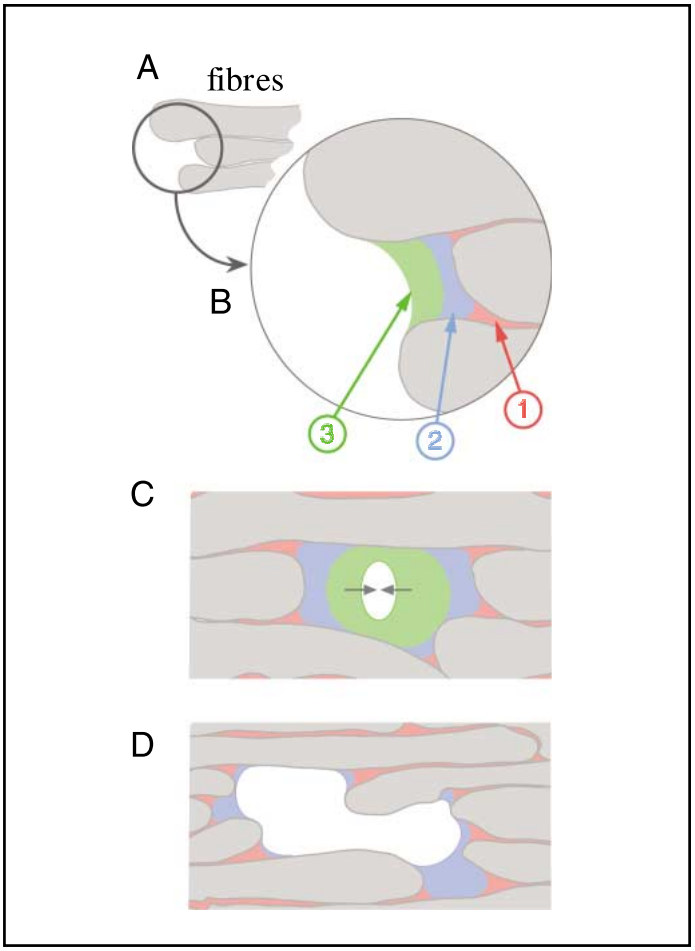

Fig. 13. (A) A schematic of a fibre cross-section with two neighbouring fibres; this leads to two fibre overlap channels being close to each other. In (B), we consider a wetting fluid configuration in 1, where the fluid fills the two fibre overlap channels and in 2, where the menisci have merged. This wetting fluid can advance down the interfibre pore as a growing collar and will stop when reaching a discontinuity within the pore 3. For a small pore (C), the advancement of one or two growing collars 2 can lead to the wetting fluid forming a film around the full circumference of the pore 3. When this occurs the pore will spontaneously fill with the wetting fluid (snap off). In (D), we illustrate a large pore which exhibits the same degree of film thickening as the small pore in (C). In this case, the same amount of film thickening leads to only partial wetting of the pore edges but no pore filling is observed (compare two pores in Fig. 7).

When discussing Fig. 7, we noted that, while the small pore (shaded red) was filled, the larger, green-shaded pore has fluid films only along the edges of the pore. This observation is completely consistent with a fluid displacement pattern mediated by film flow. Pore filling fed by films that gradually thicken, via snap off, is heavily weighted to the smaller pores; schematically, we show in Fig. 13D that a larger pore with the same film thicknesses as the pore in Fig. 13C does not form an unstable air filament and, instead, remains partially wet along the pore edges. This is what is observed experimentally in Fig. 7. The pore shaded green is very near the smaller filled red pore and would have similar film thickness. This pore, however, has not been filled completely. We observe this on a larger scale in Fig. 2 throughout the partially saturated zones, where we see smaller pores being filled, while the larger pores remain only partially wet along the edges.

It is important to note that the pores filled by a snap off (film flow) mechanism do not have to be connected to the main wetting front via filled pores. While still connected to the droplet, they are fed instead via films flowing along the dense interconnected network of fibre overlap channels. The filled (red) pore in Fig. 7 is surrounded by many unfilled pores, and can have filled only via a film flow mechanism.

This scenario, that the primary pore filling mechanism in the paper network is via fluid films, allows one to reconcile flow modelling with the experimental observations. Nearer the droplet edge, within the saturated zone (see upper left of Figs. 2,3), films along interfibre channels will be thicker; this enables even the largest pores to fill via a film-flow (snap-off) mechanism. That the filling of the pores originates from channels formed by fibre overlap, which lie almost exclusively parallel to the sheet, is consistent with the fluid configuration

observed in the saturated zone. Here, we observed the apparent pinning of the wetting fluid to the edge of the fibres and no tendency to wet the upper surface of the fibre. In the region of partial saturation, we observe the smallest pores are filled while the larger pores remain partially wet by films. Far from the droplet edge we observe the genesis of pore filling; films alone are observed.

We observe only a minimal amount of flow along the roughness of the paper fibre. In Fig. 9, we see a small film advancing down an indentation in the cellulose fibre cross-section. The advancement is very small (~10 μm) compared to the advancement along the fibre overlaps (~1 mm). This small advancement can be due to several factors. The indentation in a fibre due to collapse exhibits a large angle α which greatly reduces the driving force P_c for flow (Eq. 1). As discussed in [12], there is no simple relationship between P_c and fluid advance, so one cannot predict the relative advance along different (coupled) flow paths. However, a reduced P_c can have a significant retardation effect on the local flow mechanisms. We observe no flow down intrafibre pores; Fig. 2 exhibits no qualitative evidence of fibre swelling and, at higher magnifications (Fig. 9), we observe no flow into the fibre pits or any liquid present beneath the pits.

Relative Flow Rates Along Flow Paths

In this section, we discuss the relative flow rates one would observe along different flow pathways. From simple fluid mechanical considerations, one would expect that film flow through small channels formed by fibre overlaps, rather than meniscus displacement via bulk pores, would significantly limit the volume imbibed and the spatial extent of fluid advance into the paper sheet. Here, we show that the experimentally observed rate of penetration is in fact consistent with a film-flow process along the interfibre pores and is significantly lower than expected if the primary flow mechanism was based on meniscus flow down the bulk pores.

The prediction of two-phase liquid flow in a chaotic network of interconnected pores with channels is still an enormously challenging problem. Even studies of liquid flow along a single channel of arbitrary opening α can only be solved numerically [17].We consider first the simplest flow solution; a conventional prediction based on Lucas-Washburn theory. Here, one approximates the pores or channels as a cylindrical capillary of diameter *r*. The pressure of the wetting fluid at the paper surface is constant, and the capillary pressure in each pore is given by Laplace's equation

$$P = 2\gamma/r \qquad (2)$$

The volume flow rate q in each capillary is related to the pressure drop and the length l of imbibition of the wetting fluid along a capillary by Poiseuille's Equation, which leads to the classical result of Washburn

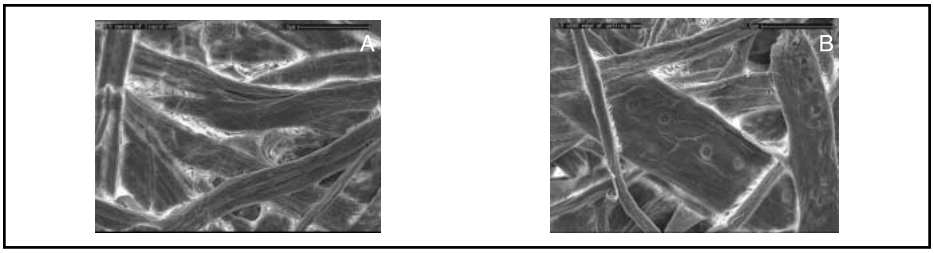

Fig. 14. Figure showing the presence of films only both near the droplet centre (A) and at the drop edge (B) after a 3 μL droplet penetrated paper.

$$l = \frac{1}{2}\left(\frac{\gamma r}{\mu}\right)^{1/2} t^{1/2} \qquad (3)$$

According to this classical result, the distance of fluid imbibition along an interfibre capillary of radius R, l_R, should be considerably further than the fluid penetration along the fibre–fibre crevice with spacing d, l_d;

$$l_R / l_d = \sqrt{R / d} \qquad (4)$$

For the paper fibre web, we have bulk interfibre pores with $R \approx 20$–50 μm. Experimentally, we assume that we are observing a dynamic snapshot of imbibition over the first second of fluid contact time. Using Eq. (3), and assuming that flow in the interfibre pores is not hindered by the presence of discontinuities, we would expect the fluid to have advanced a distance $l_R \approx$ 2–3 cm over that one second of fluid contact. This degree of advance is not observed experimentally; we observe a fluid advance of only ~1–2 mm from the drop edge in the first second of fluid contact. This observation further reinforces that flow along the interfibre pores cannot be the major flow path for the penetrating fluid.

As discontinuities hinder bulk flow, the flow of films along channels becomes most favourable. From Eq. (3) and assuming the fibre-overlap channels can be approximated by a cylinder of diameter $r \approx 1$–3 μm, one would expect the fluid advance via film flow to extend $l_d \approx$ 4–7 mm over the first second of contact. This is still faster than observed experimentally but much closer to experimental observations. A better prediction for the fluid advance down fibre- overlap channels will come from solving for the flow of the wetting phase along an edge or intersection of two planes at a crevice angle α (see Fig. 12C).

Predictions based on an hydraulic diameter approximation for flow of a wetting fluid at a sharp corner have been made previously [16]. Here we assume $\alpha = 90°$, that the pressure drop in the non-wetting phase is negligible, that the radius of curvature along the axial direction, the plane parallel to the fluid film, is very large, and that the shape of the meniscus in the cross-section is circular. The solution for this geometry is given by [16]

$$l = 0.056\left(\frac{\gamma r}{\mu}\right)^{1/2} t^{1/2} \qquad (5)$$

Equation (5) predicts a penetration depth an order of magnitude smaller than predicted by Eq. (3). For channels of $r \approx 1$–3 μm, one would expect to observe fluid advance ≈0.5–0.8 mm. This is slightly less than the extent of fluid penetration we observe experimentally. Ransohofi and Radke [17] numerically solved the full Navier-Stokes equations along a corner channel as a function of corner geometry, angle and roundedness, contact angle, and surface fluid–air shear viscosity at the gas–liquid interface. They found that the hydraulic radius method could overestimate flow resistances somewhat and also showed that flow along corners at $\alpha < 90°$ could be faster by a factor of 2–3. This result would give a prediction of l_d completely consistent with experimental observations presented herein.

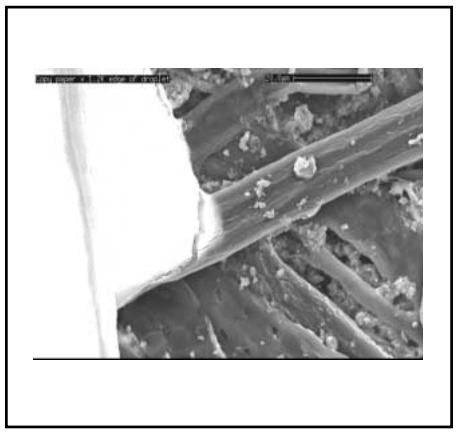

Fig. 15. Droplet edge on sized paper. No flow along channels or pores observed.

Given that the fibre overlaps form a dense network of interconnected channels, and the experimentally observed flow rate is matched accurately by a film flow scenario, it is clear that these fibre-overlap channels form the major conduits for flow in the paper fibre network.

DISCUSSION

The structure of the pore space of paper, together with local surface energy considerations, are the chief determinants of fluid penetration processes. Understanding these relationships and their implications for paper performance will help in the design of products and troubleshooting problems. In this section, we discuss the limitations of the current work and describe implications of film flow processes to industrial problems of interest to the authors.

Implications for Printing Interactions

Paper printing applications often can be described physically as a process of penetration of a finite amount of liquid into a porous structure. In most printing applications, the amount of fluid added is significantly less than that considered in the experimental section. In Fig. 14, we show examples of fluid penetration of a small droplet of 3 μL into paper. In this system, the whole droplet penetrates within ~1 s of fluid contact time. The penetration of fluid exhibits similar film flow characteristics as seen previously; one now observes no zone of complete saturation. Even in the centre of the droplet, we observe flow along interfibre channels alone and no filling of even the smallest pores. Given that many printing applications use orders of magnitude less fluid, one might expect that in many printing applications the imbibing fluid will never fill pores. This has been noted previously by Gregerson et al. [18], who studied ink distribution on and around surface fibres for flexography printed newspaper. They observed (see Fig. 10 [18]) no ink spreading into voids, but significant penetration of the surface structure via ink absorption into the interfibre voids.

We also considered the penetration of droplets onto commercial copy (sized) paper. It is thought [19] that the sizing agent preferentially sits at the intersections of fibres within sized paper; given that film flow down channels formed by fibre overlap is the preferred flow mechanism, the presence of sizing agents within channels certainly would impede the advancement of the wetting fluid. Experiments on sized paper illustrate this. In Fig. 15, we see the droplet edge on sized paper 30 s after drop application.

The fluid is not advancing and stays on the fibre surface – no channel flow is observed. As channel flow is the major mechanism for fluid imbibition, this may give an indication as to why sizing agents are so effective.

Viscous Effects

In all the cases we have considered experimentally, penetration is determined by capillary forces. Fluid penetration will be strongly affected if fluid is applied to the sheet under pressure (e.g. printing nip). One would in this case expect the wetting fluid to be driven down the pores. However, when pressure is released, capillary transport will again dominate the flow mechanisms, and any excess fluid and fluid within pores will continue to penetrate via films. We will discuss the role of different pressure states and the effect on fluid transport in another paper.

Implications for Fluid Distributions Within Sheets

Flow along channels and the filling of pores away from the wetting front has a dramatic effect on the resultant fluid phase distribution. As we are particularly interested in the optimization of resin penetration into decor paper, this is of great interest. We have performed experiments on a range of industrial decor papers which exhibit a wide range of pore structure and vary in their fibre and filler content. The fluid penetration observed is similar to that shown previously for pure cellulose paper (see Fig. 16). Flow down the interfibre channels and partially filled pores are all evident.

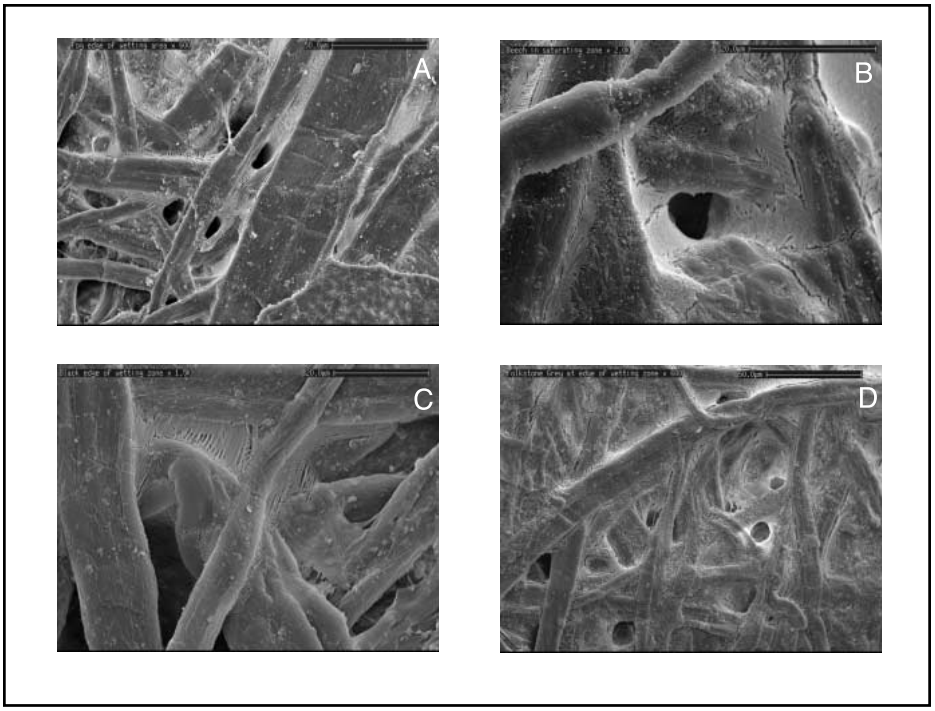

Fig. 16. Images of fluid penetration into decor papers (A) fog, (B) beech, (C) black and (D) Folkstone grey. All exhibit penetration patterns similar to those observed in the fully bleached softwood kraft paper.

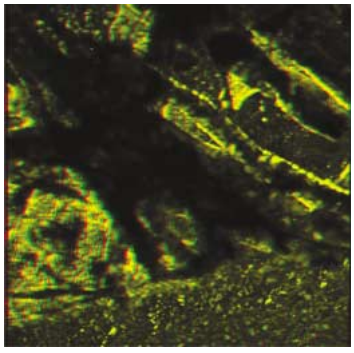

Fig. 17. Cryogenic 2-photon image of fluid penetration into papers directly beyond the droplet the edge of which can be seen in the bottom quarter of the image. It is a stereo pair which can be viewed using green and red anaglyphic glasses.

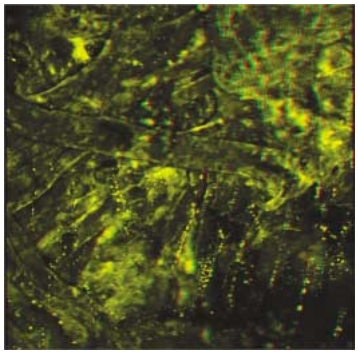

Fig. 18. Cryogenic 2-photon image of fluid penetration into papers directly underneath the droplet clearly showing interfibre film flow and voids. Note that the presence of bulk liquid in the droplet over the fibre can be seen by the fluorescent dots that appear closer to the viewer.

ACKNOWLEDGEMENTS

The authors wish to thank Dr. Roger Heady of the ANU Electron Microscopy Unit for assistance with the imaging study. Tim Senden thanks the ARC for support through an Australian Research Fellowship.

NOTE

Since submission, a detailed study has been completed using cryogenic two-photon laser confocal microscopy: this method enables one to obtain 3-D images of fluid penetration at arbitrary depths and below the droplet. Interfibre channel flow is observed under the films in the saturated zone near the droplet edge (Fig. 17). Interfibre channel flow and unfilled void spaces are also observed directly underneath the droplet (Fig. 18). This result, which is part of a paper recently submitted for publication, confirms that the primary mechanism for fluid penetration into unsized paper, both at the edge of the droplet and directly under the drop, is via flow along interfibre channels.

REFERENCES

1. LUCAS, R., "Ueber das Zeitgesetz des kapillaren Aufstiegs von Fleussigkeiten", *Kolloid Zeitschrift* 23:15–22 (1918).

2. WASHBURN, E.W., "The Dynamics of Capillary Flow", *Physical Review* 17:273–283 (1921).
3. KENT, H. J. and LYNE, M.B., "Influence of Paper Morphology on Short Term Wetting and Sorption Phenomena" in Fundamentals of Papermaking, C.F. Baker, Ed., Mech. Eng. Publ. Ltd., 895–920 (1989).
4. MARMUR, A., "Drop Penetration into a Thin Porous Medium", *J. Coll. Interface Sci*. 123:161 (1988).
5. LARSON, R., SCRIVEN, L.E., and DAVIS, H.T., "Percolation Theory of Residual Phases in Porous Media", *Nature* 268:409–413 (1977).
6. LINDQUIST, B., LEE, S.M. and COKER, D., "Medial Axis Analysis of Void Structure in Three-Dimensional Tomographic Images of Porous Media", *J. Geophys. Res.* 101B:8297–8310 (1996).
7. LINDQUIST, W.B., VENSKATARANGAN, A., DUNSMUIR, J. and WONG, T.F., "Pore and Throat Size Distributions Measured from Synchrotron X-Ray Tomographic Images of Fontainbleau Sandstones", *J. Geophys. Res.* 105B:21508 (2000).
8. SOK, R.M., KNACKSTEDT, M.A., SHEPPARD, A.P., PINCZEWSKI, W., LINDQUIST, W.B., VENSKATARANGAN, A. and PATERSON, L., "Direct and Stochastic Generation of Network Models from Tomographic Images; Effect of Topology on Two Phase Flow Properties", *Transport in Porous Media* 46:345–371 (2002).
9. GOEL, A., TZANAKAKIS, M., HUANG, S., RAMASWAMY, S., CHOI, D., and RAMAROA, B.V., "Characterization of the Three-Dimensional Structure of Paper Using X-Ray Microtomography", *Tappi J.* 84(5) (2001).
10. EKLUND, D. and SALMINEM, P., "Water Sorption in Paper During Short Times", *Appita J.* 40(5):340–346 (1987).
11. SCHOELKOPF, J., GANE, P.A.C., RIDGWAY, C.J. and MATHEWS G.P., "Influence of Inertia on Liquid Adsorption into Paper Coating Structures", *Nordic Pulp Paper J.* 15(5):422–430 (2000).
12. SENDEN, T.J., KNACKSTEDT, M.A. and LYNE, M.B., "Droplet Penetration into Porous Networks: Role of Pore Morphology", *Nordic Pulp Paper J.* 15(5):554–563 (2000).
13. ROBARDS, A.W. and SLEYTR, U.B., "Low Temperature Methods in Biological Electron Microscopy" in Practical Methods in Electron Microscopy, Vol. 10, Elsevier, Amsterdam, The Netherlands (1985).
14. HASUIKE, M., KAWASAKI, T. and MURAKAMI, K. "Evaluation Method of 3D Geometric Structure of Paper Sheet", *J. Pulp Paper Sci.* 18(3):J114–J120 (1992).
15. SAMUELSON, E.J., GREGERSON, O.W., HOUEN, P.J., HELLE, T., RAVEN, C. and SNIGIREV, A., "Three-Dimensional Imaging of Paper by Use of Synchrotron X-Ray Microtomography", *J. Pulp Paper Sci.* 27(2):50–53 (2001).
16. LENORMAND, R., ZARCONE, C. and SARR, A., "Mechanisms of the Displacement of One Fluid by Another in a Network of Capillary Ducts", *J. Fluid Mech.* 135:337–353 (1983).
17. RANSOHOFF, T.C. and RADKE, C.J., "Laminar Flow of a Wetting Fluid Along the Corners of a Predominantly Gas-Occupied Noncircular Pore", *J. Colloid Interface Sci.* 121:392–401 (1987).
18. GREGERSON, W., JOHNSON, P.O. and HELLE, T., "Small Scale Topographical Variations of Paper Surfaces, and Their Effects on Printing Ink Transfer Distribution", *J. Pulp Paper Sci.* 21(10):J331–J336 (1995).
19. GARNIER, G., BERTIN, M. and SMRCKOVA, M., "Wetting Dynamics of Alkyl Ketene Dimer on Cellulosic Model Surfaces", *Langmuir* 15:7863–7869 (1999).

REFERENCE: ROBERTS, R.J., SENDEN, T.J., KNACKSTEDT, M.A. and LYNE, M.B., Spreading of Aqueous Liquids in Unsized Papers is by Film Flow, Journal of Pulp and Paper Science, 29(4):123–131 April 2003. Paper offered as a contribution to the Journal of Pulp and Paper Science. Not to be reproduced without permission from the Pulp and Paper Technical Association of Canada. Manuscript received November 20, 2001; revised manuscript approved for publication by the Review Panel December 12, 2002.

KEYWORDS: KRAFT PAPERS, BLEACHED PULPS, KRAFT PULPS, SOFTWOODS, WATER BASED FORMULATIONS, FLUID FLOW, PENETRATION, PAPER FIBRE, POROUS MEDIA, CAPILLARITY.